

RESEARCH

Open Access



Optimization of intranasal bleomycin dose for effective pulmonary fibrosis induction in mice with minimal animal distress

Anita Salmaso¹, Anna Valeria Samarelli^{2,3}, Giulia Yuri Moscatiello¹, Giulia Raineri^{3,4}, Alfredo Cagnotto⁵, Paolo Bigini¹, Enrico Clini^{2,3}, Roberto Tonelli^{2,3} and Annalisa Morelli^{1*}

Abstract

Background Pulmonary fibrosis is a progressive interstitial lung disease driven by aberrant alveolar epithelial repair and dysregulated crosstalk with mesenchymal cells, leading to myofibroblast activation and excessive extracellular matrix deposition. Current mouse models for studying its pathogenesis often use invasive methods like intratracheal bleomycin administration, which can cause significant animal distress. This study aims to refine the bleomycin model via intranasal instillation, reducing animal suffering while improving reproducibility and translational value.

Methods The MALDI-TOF MS analysis allowed for the identification of the spatial distribution of bleomycin directly on the lung tissue of C57BL/6 J mice after intranasal administration to demonstrate the effectiveness of this route. Different doses (1, 3, 5 mg/kg) of bleomycin were tested in mice. Non-invasive whole-body plethysmography enabled the monitoring of the disease progression and the assessment of pulmonary function in conscious mice. Histopathological analyses were performed to follow fibrosis progression.

Results This method resulted in impaired respiratory function, with a similar pattern observed for both 5 and 3 mg/kg doses. Histopathological evaluations revealed rapid acute inflammation followed by chronic fibrosis in both dosage groups, similar to human IPF. Key molecular markers (CD68 and COL 1a1) were upregulated in response to the treatment, with similar expression patterns between the two doses, suggesting an inflammatory response and established fibrosis. 1 mg/kg dosage did not lead to any relevant clinical changes and was therefore excluded from further analyses.

Conclusions Intranasal administration proved to be an efficient technique, delivering a uniform bleomycin distribution in the lungs. Bleomycin instillation induced lung injury and fibrosis comparable to those achieved with the conventional intratracheal protocol, both histologically and functionally, while reducing invasiveness and animal distress. The optimal bleomycin dosage was determined to be 3 mg/kg, which induced a similar level of respiratory distress, but with less weight loss and reduced risk of mortality. This approach provides a reproducible model for preclinical studies of pulmonary fibrosis. This strategy ensures consistent and reproducible scientific data, pivotal for bridging the gap between benchside and bedside.

*Correspondence:
Annalisa Morelli
annalisa.morelli@marionegri.it

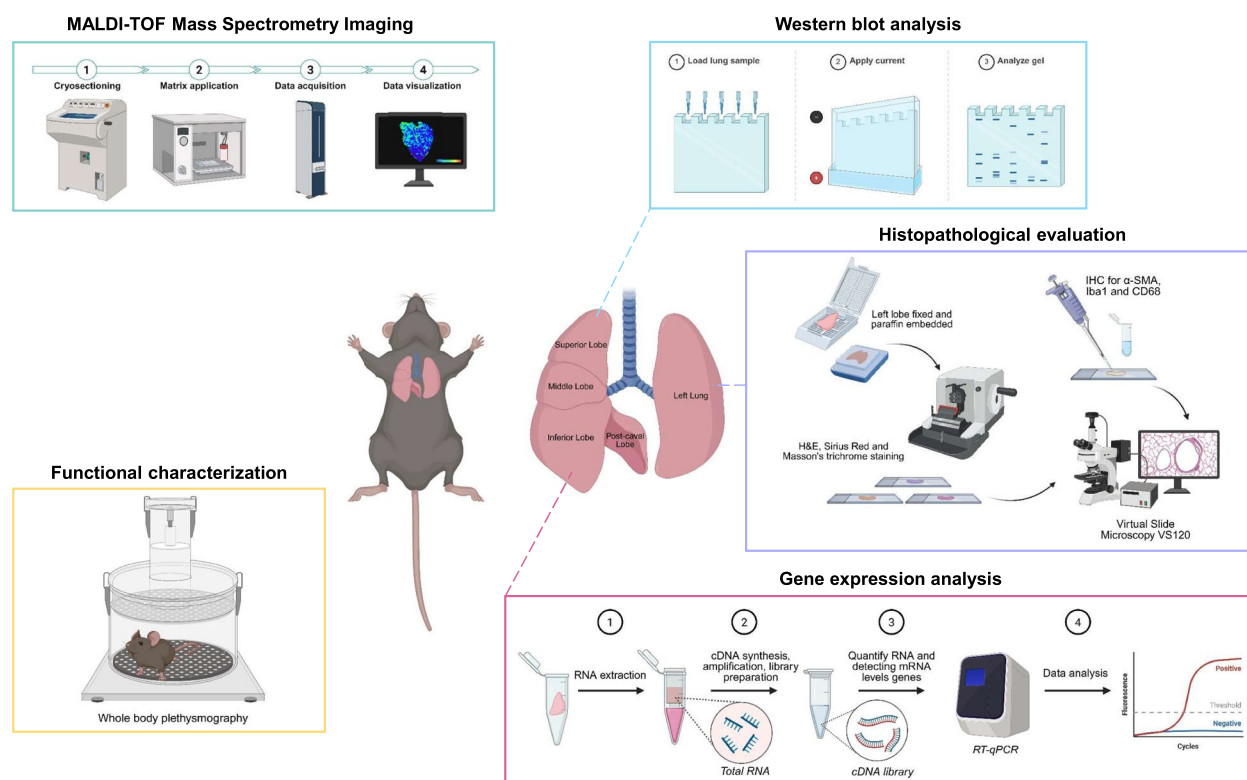
Full list of author information is available at the end of the article



© The Author(s) 2025. **Open Access** This article is licensed under a Creative Commons Attribution-NonCommercial-NoDerivatives 4.0 International License, which permits any non-commercial use, sharing, distribution and reproduction in any medium or format, as long as you give appropriate credit to the original author(s) and the source, provide a link to the Creative Commons licence, and indicate if you modified the licensed material. You do not have permission under this licence to share adapted material derived from this article or parts of it. The images or other third party material in this article are included in the article's Creative Commons licence, unless indicated otherwise in a credit line to the material. If material is not included in the article's Creative Commons licence and your intended use is not permitted by statutory regulation or exceeds the permitted use, you will need to obtain permission directly from the copyright holder. To view a copy of this licence, visit <http://creativecommons.org/licenses/by-nc-nd/4.0/>.

Keywords Intranasal delivery, Pulmonary fibrosis, Inflammation, Histopathology, Plethysmography

Graphical abstract



Introduction

Pulmonary fibrosis (PF) is a chronic and progressive condition that belongs to the interstitial lung diseases (ILDs), accounting for about 200 different pathologies [1]. The pathogenesis involves a complex interplay of different cell types, such as alveolar epithelial cells, lung fibroblasts, and the innate and adaptive immune system. Indeed, the precise mechanisms underlying the relationship of these factors in disease development remain elusive [2, 3]. However, it has been shown that an aberrant tissue repair response leads to a progressive deposition of extracellular matrix (ECM), alveolar destruction, irreversible scarring, and loss of pulmonary function [4, 5]. Idiopathic pulmonary fibrosis (IPF) is the most common form of ILD, whose incidence ranges from 3 to 9 cases per 100,000 per year in Europe and North America [6]. Among the animal models historically employed to recapitulate the human fibrotic progression (radiation exposure, silica or asbestos, fluorescein isothiocyanate and transgenic mice or gene transfer employing fibrogenic cytokine [7–10]), the bleomycin (BLM)-induced animal model represents one of the most widely used due to its ability to mimic several aspects of human fibrotic lung disease [11–13].

BLM, a glycopeptide antibiotic and antineoplastic agent, exerts its effects through the generation of reactive oxygen species [14] and is primarily used in clinics for the treatment of various carcinomas and lymphomas [15, 16]. Although in preclinical settings the induction of fibrosis by BLM has been widely reported in the literature [13, 17], some controversies remain [18]. Furthermore, preclinical studies have employed a wide range of BLM doses, without standardization of the induction of the mouse model of IPF, and often producing variable outcomes [19]. Additionally, to induce IPF, BLM can be administered by various routes, and the most frequently used method is intratracheal (IT) administration. However, its clinical relevance remains a subject of debate, as it represents the most potent stimulus. Still, it is extremely invasive, leading to injury to the trachea caused by needle insertion and signs of inflammation in healthy mice undergoing IT. The main concern was the higher inter-subject variability in some outcomes, especially respiratory parameters, caused by the relative differences based on the operator performing the procedure. Indeed, while IT administration is well-documented, it poses more technical challenges and requires staff training [20–22].

Alternative approaches should therefore be undertaken to minimize the number of animals used and their suffering during procedures, while maintaining symptom reproducibility and the generation of reliable scientific data. The modulation of the protocol of induction offers the possibility of a broader range of injuries that mirror human clinical patterns [23]. Moreover, different administration routes require proper dosage, anesthetic agents, invasiveness, and technical difficulties that influence the amount of drug delivered to the lungs. Selecting the most suitable, feasible, and tolerable protocol, in line with the ethical principles of animal welfare and the preclinical translation, is crucial. To this aim, the ability to generate IPF by intranasal (IN) routes has been investigated. Since IN is not the gold standard for inducing IPF in animal models, performing Matrix-Assisted Laser Desorption/Ionization Time-of-Flight Mass Spectrometry (MALDI-TOF MS), a powerful tool for drug distribution studies [24], would be essential to explore the spatial distribution of BLM and confirm its lung-specific deposition. The Refinement and the Reduction of the 3Rs principles can be combined with the inclusion of non-invasive methods, which enable the researchers to monitor the clinical progression, or the effect of a treatment in mice, by techniques closely associated with those used in the management of IPF patients. In this context, it is important to examine the correlation between BLM administration and the functional respiratory response by linking changes in respiratory patterns with histological evidence of damage progression, obtaining a multimodal approach. Among the different strategies, the whole-body barometric plethysmography, a non-invasive tool, detects changes in respiratory functions following the disease progression and permits the determination of longitudinal lung physiology without inducing excessive distress in animals [25]. Integrating distribution and spatial studies with non-invasive functional analysis and histopathological evaluation enables a comprehensive characterization of the model, enhancing its translatability to clinical practice. This research paper is based on these premises to establish a reliable model for evaluating future innovative therapeutic strategies.

Materials and methods

Bleomycin-induced pulmonary fibrosis in mice and treatment

12-week-old male C57BL/6 J mice were purchased from Charles River Laboratories (Calco, LC), housed in a pathogen-free sterile facility at the Mario Negri Institute for Pharmacological Research IRCCS, and allowed water and food ad libitum. All experiments were approved by the IRCCS-IRFMN Animal Care and Use Committee (IACUC) and subsequently approved by the Italian “Istituto Superiore di Sanità”.

For the evaluation of the short-term spatial distribution of BLM in the lungs performed with MALDI-TOF MS, 6 mice were anesthetized by intraperitoneal injection of 0.4 mg/kg medetomidine (Domitor®) and 36 mg/kg ketamine (Lobotor®) and treated with 5 mg/kg Bleomycin sulfate (TCI, Tokyo) and sacrificed 30 min, 2 h and 6 h post nasal instillation.

For the evaluation of fibrosis progression through IN administration, mice were anesthetized by intraperitoneal injection of 0.4 mg/kg medetomidine (Domitor®) and 36 mg/kg ketamine (Lobotor®). For the first experiment, 20 mice were treated with 5 mg/kg Bleomycin sulfate (TCI, Tokyo), while 5 mice received a vehicle (0.9% saline). In the second experiment, 20 mice were treated with 3 mg/kg Bleomycin sulfate (TCI, Tokyo), while 5 mice received a vehicle (0.9% saline). In the last experiment, 20 mice were treated with 1 mg/kg Bleomycin sulfate (TCI, Tokyo), while 5 mice received a vehicle (0.9% saline). Bleomycin was instilled via a micropipette, 25 µl per nostril, with a total volume of 50 µl. Animals were allowed to recover immediately afterward (Antisedan®—0.8 mg/kg intraperitoneally). Bodyweight and survival were monitored. The animals were treated with BLM at day 0, representing the baseline, and euthanized by decapitation ($n = 4–5$ for each time point) at 7, 14, 21, and 28 days post-administration.

MALDI-TOF MS analysis

Following IN treatment with BLM, mice were sacrificed at different time points: 30 min, 2 h, and 6 h. The lung, stomach, and small intestine of mice were excised, rapidly washed in saline, directly frozen in liquid nitrogen, and stored at -80°C before sectioning. Cryogenic Sects. (16 µm thick) were prepared at -20°C in a cryostat (Leica Microsystem, Italy), mounted in a MALDI targets plate (Applied Biosystem) using a small brush, and placed under vacuum at 4°C overnight. Subsequently, samples were stored at -20°C until use. On the day of the experiment, plate-mounted tissue sections were coated with a matrix solution of α -Cyano-4-hydroxycinnamic acid (HCCA, 15 mg/ml) dissolved in 60% acetonitrile/0.2% trifluoroacetic acid using a glass nebulizer. The plate was dried at room temperature and finally was inserted into a MALDI-TOF MS (4800 MALDI-TOF, Applied Biosystem). For a correct identification of BLM distribution, the same solution used for treatment was used as external standard for generating MALDI-TOF mouse tissue imaging. The analysis was carried out in positive ionization reflector mode, and the scan range was set to m/z from 1400 to 1600 with a raster of 120 µm. The raw data were converted into images using the TissueView software.

Plethysmography analysis

The non-invasive whole-body plethysmograph consists of two chambers, a ventilation pump, a differential pressure transducer connected to an amplifier, and a 10-ml calibration syringe inserted at the other end of the chamber. The ventilation pumps and pneumotachographs allow air renewal inside the plethysmograph (Vent4, Emka Technologies). The pressure transducer measured the pressure difference between the subject chamber and the reference chamber. This signal was then amplified (usb-AMP; Emka Technologies), analyzed with a respiratory flow analyzer module, and recorded with a data recording program (Iox acquisition software, ver. 2.8, Emka Technologies) using a standard desktop PC. Each mouse was put inside the chamber, ensuring the animal was properly restrained. To minimize the effects of stress, animals were allowed to stay in the restraining system the day before BLM administration. The experiment provides baseline recording lasting for 3 min, followed by a recording session of 5 min (final values are expressed as the average of measurements acquired every 10 s). For data acquisition, the lung function was analyzed at weekly intervals on days 7, 14, 21, and 28 post BLM challenge, and data for the same animal were collected over different week intervals. The respiratory parameters of respiratory rate (RR, breaths/min), inspiratory time (Ti, msec) and expiratory time (Te, msec), peak inspiratory flow (PIF, ml/sec), and peak expiratory flow (PEF, ml/sec) were derived directly from the respiratory traces. For the tidal volume (Vt, ml), the integral of the Ti value obtained from the respiratory trace was calculated. Once Vt had been determined, minute volume (VE, ml; Vt x RR) and the ratio of inspiration time to expiration time (Ti/Te ratio) were also calculated.

Tissue collection and histological analysis

Lungs from BLM-treated animals were fixed in 10% formalin for 24 h (Bio-Optica) and paraffin-embedded, followed by cutting with Leica RM55 microtome (Leica Microsystems, Italy) into 4 µm-thick sections. Slices were deparaffinized in xylene and rehydrated through a series of alcohols to water. The Hematoxylin–Eosin (H&E – Bio-Optica) staining method assessed inflammation and fibrosis. Picrosirius Red (0.5 g Sirius Red F3B (C.I. 35,782) + 500 ml picric acid solution – Sigma Aldrich) and Masson's trichrome (Trichrome stain kit HT15-KT—Sigma Aldrich) staining to reveal collagen were performed following manufacturer's instructions. Paraffin-embedded sections were immunoassayed using Vectastain Elite ABC (Vector Laboratories, Burlingame, CA, USA). Antigen retrieval was performed in citrate buffer (pH 6) in a boiling pot for 15 min, endogenous peroxidase inhibition with H₂O₂ 3% for 10 min, and incubation with blocking solution (Phosphate buffer-Normal Goat Serum, PBS-NGS 10%-Tween 20 0.05%)

for 30 min. Ionized calcium-binding adaptor molecule 1 (Iba1—clone 019–19741, Wako; 1:500) was used to label macrophage calcium-binding protein and Alpha Smooth Muscle Actin (α-SMA—Thermo Fischer Scientific, 1:100) for myofibroblast, incubated overnight at 4 °C. Sections were stained with 3,3–Diaminobenzidine (DAB, Sigma Aldrich) and counterstained with Mayer's Hematoxylin (Bio-Optica). All the samples were dehydrated through an alcohol scale and mounted with DPX (Sigma Aldrich). For immunofluorescence analysis, lung cryostat sections were cut at 20 µm, post-fixed in 10% formalin (Bio-Optica) for 20 min, washed in PBS for 5 min, and incubated for 1 h with a blocking solution (PBS-NGS 10%-Triton X-100 0.1%). For subcellular localization, primary rat anti-CD68 monoclonal antibody (1:200, Serotec, Kidlington, UK) + Triton X-100 0.1% + NGS 3% in 1X PBS overnight at 4 °C was used. Slides were incubated with the Alexa488 conjugated secondary antibody (1:500, Invitrogen) for 1 h in 1% 1X-NGS PBS solution and then with the Hoechst nuclear marker 33,258 (2 µg/mL in 1X PBS, Sigma Aldrich) for 10 min. Fluoromount Aqueous Mounting Medium (Sigma Aldrich) was used for mounting with a cover glass. The slides were observed at the Virtual Slide Microscopy VS120 (Olympus, Japan). For the Quantification of α-SMA and CD68 signal analyses methods, see Supplementary Information (S.I.).

Quantification of collagen deposition and lung damage

For collagen fiber quantification, Sirius Red-stained sections were analyzed in blind (*n*=3). The percentage of collagen deposition area was determined using ImageJ software. Fibrotic changes in each lung section were assessed as the mean of the severity scores obtained from observed microscopic fields. 24 random fields of view were manually selected and observed with an objective lens magnification at 20X. Original images were converted into RGB images, providing grayscale pictures for the red, blue, and green channels separately. For the greyscale image corresponding to the green channel, the threshold was manually adjusted until the entire green area was highlighted in red, and the pixel of the detected regions was measured using the measure tool [26]. For the determination of lung damage, Masson's trichrome-stained sections were analyzed in a blinded way (*n*=3). Scores from 0 (normal) to 8 (total fibrosis) were assigned according to the predetermined Ashcroft scale [27, 28]. After examination, the mean of the scores from all fields was taken as the fibrotic score.

Quantitative real-time polymerase chain reaction

Total lung RNA was isolated with TRIzol Reagent (Thermo Fischer Scientific) according to the manufacturer's instructions, and 1 µg total RNA was reverse transcribed into cDNA using a high-capacity cDNA reverse

transcription kit (Applied Biosystems). cDNAs were mixed with Quantifast SYBR Green Master Mix (Bio-techRabbit) according to the manufacturer's instructions, and both forward and reverse primers (0.5 μM) for detecting mRNA levels of mouse genes. qPCR was carried out using QuantStudio 5 Systems (Applied Biosystems), and the amplification steps were 50 °C for 2 min, 95 °C for 10 min, followed by 40 cycles of 95 °C for 15 s and 60 °C for 1 min. Relative mRNA levels of the target genes were normalized to β-ACT mRNA expression and analyzed by the 2^{-ΔΔCt} method. Quantitative Reverse-Transcriptase PCR (RT-PCR) primers are reported in Table 1.

Isolation of total proteins from mouse lungs and Western Blot analysis

Frozen mouse lung tissues (25 mg; 2–4 mice per condition) were processed with lysis buffer (A45735 easy pep lysis buffer from easy pep mini ms sample prep kit, a40006, ThermoFisher, USA) using the OctoMACS™ Dissociator (Miltenyi Biotec) through the Protein_01_01 program, according to the manufacturer's instructions. Then, the M-Tubes were centrifuged at 900 rcf for 5 min, and the supernatants were centrifuged for 10 min at 16.000 rcf. Then, the supernatants containing the extracted proteins were quantified with BCA protein assay kit (cod. 23,227, Pierce™ BCA Protein Assay Kit, Thermo Scientific, USA), which was a detergent-compatible formulation (after the dilution 1:10 of samples), and the protein standards were prepared using the same lysis buffer as the samples. Western blot (WB) analysis was performed according to standard protocols. Briefly, 35 μg of total protein lysate was separated by SDS-PAGE gel electrophoresis. Then, proteins were transferred to a nitrocellulose membrane, and primary antibodies Anti-SMAD2/3 (D7G7) (1:1000, cod. 8685, Cell Signaling, MA, USA), Anti-Phospho-Smad2 (pSMAD 2, 1:1000, cod. 3108, Cell Signaling, MA, USA) and Anti-Vinculin (1:1000, cod. Ab207440, Abcam, USA) were incubated overnight at 4 °C. After the incubation of the membranes for 1 h at room temperature with horseradish peroxidase-conjugated anti-rabbit secondary antibodies (1:30.000; cod. A120-101P, Bethyl, MA, USA), followed by the incubation with the ECL (Pierce ECL, cod. 32,209, Thermo Scientific, USA), specific protein bands were revealed. To ensure consistency in data presentation, the blot

containing both BLM doses (3 and 5 mg/kg) was split in the Results section. The unedited original blot is available in the S.I. (Figure S2).

Data calculation and statistical analysis

All statistical analyses were performed using GraphPad Prism version 10 for Windows (GraphPad Software, CA, USA). All data are expressed as mean ± standard error of the mean (SE). For the bodyweight and weight loss, Two-Way ANOVA followed by Šidák's test was performed. For the plethysmography analysis, we considered only the animals that reached the final time point (28 days after BLM administration), excluding those from the groups randomly sacrificed at earlier time points (7, 14, and 21 days after BLM administration) for histopathological analysis. Non-parametric Mann–Whitney U test was used to compare lung function parameters with the CTR group at each time point. For the histopathological and molecular biology analysis, the differences between groups were compared using Kruskal–Wallis test followed by Dunn's test. Non-Parametric One-Way ANOVA was used to determine the statistical significance of the intensity bands from WB. P values < 0.05 were considered statistically significant and reported on graphs. For in vivo experiments, the number of animals sacrificed at each data point was minimized according to the 3Rs principle.

Results

MALDI-TOF MS analysis showed lung deposition and distribution of BLM after IN administration

To evaluate the relevance of the IN administration route for inducing IPF, 6 twelve-week-old C57BL/6 J male mice received a single IN instillation of BLM at 5 mg/kg in 50 μl. Quantification of BLM in murine biological tissue was performed after MALDI-TOF calibration with the same BLM solution used for the treatment.

Figure 1A shows that the BLM signal intensity follows a linear trend in the concentration range from 0.01 to 1 μg/μl, also confirming that there is no reduction in the BLM signal in the presence of biological tissue (lung). The spectrum confirmed a 90% purity of the BLM solution used for treatment (Fig. 1A – lower panel).

Tissue from saline-treated control animals exhibited the same background value as shown in the CTR image. MALDI imaging demonstrated that BLM reached the lung following IN instillation. 30 min post-administration, a detectable drug signal was already present in the peripheral lung regions. By 2 h, the signal had diffused throughout the lung parenchyma. Detectable levels of BLM persisted within the lung up to 6 h post-administration. Analysis of gastrointestinal tissue revealed the early presence of BLM in the stomach at 30 min. In contrast, the small intestine showed a delayed kinetic

Table 1 RT-PCR primer sequences

	5'- 3' Forward	5'- 3' Reverse
β-ACT	GCCTGAGGCTCTTTTCCAG	TGCCACAGGATTCATACCC
TNF-α	AGACCCTCACACTCAGAT-CATCTTC	TTGCTACGACGTGGGCTACA
COL 1a1	ACCTGTGTGTTCCCTACTCA	GACTGTTGCCCTCGCCTCTG
FN1	CACGGAGGCCACCATTA	CTTCAGGGCAATGACGTAGAT

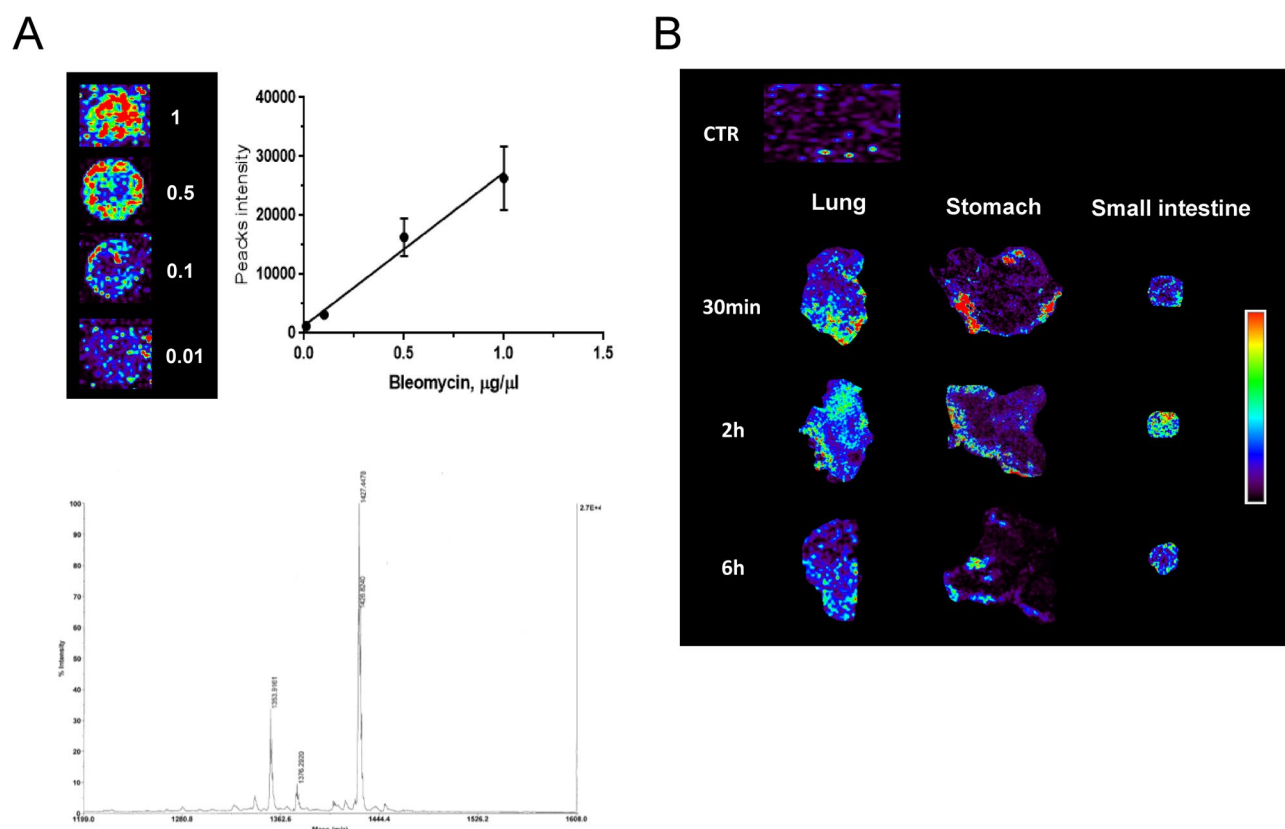


Fig. 1 MALDI-TOF images of BLM distribution in mouse biological tissues. **A** Linear regression obtained with different concentrations of BLM (1, 0.5, 0.1, 0.01 µg/µl) spotted on CTR lung tissue section and acquired with the same conditions used for the tissue sections (upper panel). Representative spectrum with the indication of the molecular weight of the BLM solution (lower panel). **B** Representative images of BLM distribution in the mouse lung, stomach, and small intestine at different time points after treatment. The colored bar on the side indicates the concentration of BLM in the different biological tissues: blue for the lowest concentration, red for the highest concentration. The biological tissue background of the saline-treated mouse is indicated as CTR

profile, with predominant BLM signal emerging at 2 h post-instillation. Notably, both the stomach and small intestine exhibited no diffuse signal at the final time point (Fig. 1B).

Poorly invasive intranasal administration of BLM induced a reliable induction of IPF in C57BL/6 J-treated mice

The study was conducted in 20 twelve-week-old C57BL/6 J male mice receiving a single IN instillation of BLM (5 mg/kg) or 4 with the same volume of sterile saline solution under ketamine/medetomidine anesthesia. BLM directly penetrating from the nostrils and rapidly moving through the larynx, tracheal duct, and bronchus was able to deeply impact, inducing a weight loss of 30% in the first two weeks, followed by slow weight recovery (Fig. 2A, B). Since BLM-treated animals also showed typical signs of general distress, such as marked piloerection, hunched posture, and inactivity, more specific parameters ascribable to pulmonary deficit were evaluated by plethysmography analyses (Fig. 2C–J). In BLM-treated mice, the T_i exhibited a significant gradual increase following administration,

consistently surpassing that of the control group throughout the study period (Fig. 2C). Fibrotic mice showed a significant increase in T_e by day 7 post-treatment, which subsequently decreased gradually to levels comparable to the controls by day 21 (Fig. 2D). BLM demonstrated a depressive effect on the chrono component of respiratory drive, evidenced by a persistent and gradual increase in T_i , accompanied by a rapid rise in T_e , and subsequent normalization of the expiratory cycle. Interestingly, BLM-treated animals exhibited a marked increase in V_t from 0.16 to 0.28 by day 7 (Fig. 2E), accompanied by a similar trend in V_E (Fig. 2F). This increase may be attributed to prolonged T_i and/or heightened breathing effort caused by BLM-induced acute lung damage. As expected, the RR decreased in the BLM-treated mice, persistently maintaining a significantly lower level compared to the controls (Fig. 2G). This reduction is primarily due to changes in lung mechanics and compensatory adjustments. It clarifies the deep association between the three parameters and their reliability in elucidating a respiratory discomfort typical of IPF. In Fig. 2

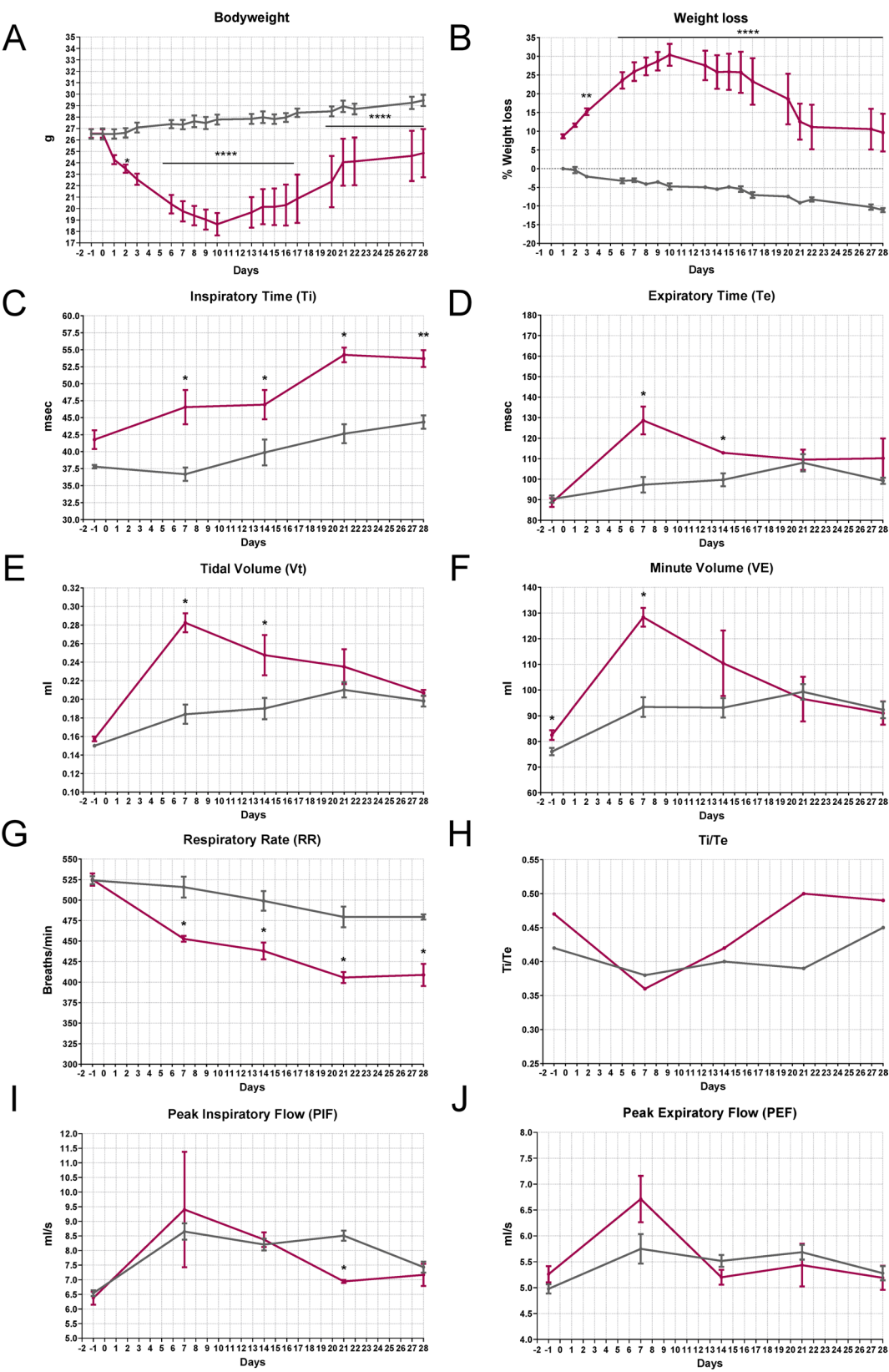


Fig. 2 (See legend on next page.)

(See figure on previous page.)

Fig. 2 Health status in BLM-induced lung injury mouse model—Plethysmography (IN—5 mg/kg). **A** Bodyweight and **B** weight loss in C57BL/6 J mice treated via single IN administration with BLM (red line) or vehicle (grey line). The data were analyzed using Two-Way ANOVA followed by Šidák's test. * $p \leq 0.05$, ** $p \leq 0.01$, *** $p \leq 0.0001$. **C–J** Effect of BLM on Ti (msec), Te (msec), Vt (ml), VE (ml), RR (breaths/min), Ti/Te, PIF (ml/s), and PEF (ml/s) in C57BL/6 J mice. Control animals are represented by the grey line ($n=5$); BLM-treated animals are represented by the red line ($n=4$). Data are reported as mean \pm SE. The data were analyzed using the non-parametric Mann–Whitney U test comparing the parameters with the CTR group at each time point, * $p \leq 0.05$, ** $p \leq 0.01$

(H–J), the trends of Ti/Te, PIF, and PEF showed no differences between the two groups. This outcome was expected, as these parameters typically change in the presence of major airway obstruction [29]. In IPF, airway involvement occurs primarily at the level of small airways, with evidence of air trapping when going from functional residual capacity to residual volume [30, 31].

A deep investigation of lung tissues at different time points has been undertaken to make a correlation between clinical and pathological features characterizing IPF models. Histological evaluation by H&E staining revealed a slight to moderate infiltration of inflammatory cells, including macrophages and neutrophils, at 7 days post-instillation, indicating an initial lung injury and acute inflammation (Fig. 3A). During disease progression, a rapid infiltration of cells into the lung parenchyma is observed. This infiltration did not present a homogeneous diffusion but is rather characterized by areas of high infiltration, interspersed with areas in which the cytoarchitecture is maintained. This pattern of alteration is consistent with the BLM model already described and also recapitulates some aspects of acute inflammation that can be detected by radio-diagnostic in patients. Over time, despite no repeated BLM inhalations, the migration of circulating cells into the lungs increases, peaking between days 14–21 post-treatment (Fig. 3A, H&E panel—arrows). At the end of the follow-up, at 28 days after BLM instillation, the lung parenchyma appears less congested, which is consistent with the type of insult and with the high capacity to respond in young animals.

To better characterize the cellular composition and lung infiltrates, immunohistochemical analysis for Iba1, a marker of alveolar, interstitial, and circulating macrophages, and CD68, a marker of macrophage lysosomes, was performed. Macrophage infiltration into the lungs was significantly greater in the BLM group as compared to the controls, at 7, 14, and 21 days (Fig. 3B). Notably, positive cells for both macrophage markers showed an irregular shape, indicating their activated state compared to the round shape in the control group. We proceeded to investigate the alveolar fibrosis with two markers, Sirius Red and Masson's trichrome, on serial sections (Fig. 3A). Both stainings showed severe expanded alveolar and interstitial fibrosis and abnormal collagen deposition. PF and disruption of normal lung architecture

occurred particularly from 14 to 28 days (Fig. 3A—Sirius Red panel—arrows). Masson's trichrome distinguishes between pre-existing collagen fibers (in dark blue) from those in neoformation (in light blue). Two different quantitative parameters were analyzed using ImageJ software to assess the extent of fibrosis: collagen deposition and the percentage of positive Sirius Red staining. As shown in Fig. 3C, the collagen deposition quantification revealed no difference at 7 days compared to the control group. This confirmed that the inflammatory phase occurs in the first week post BLM administration, where ECM is not yet highly produced. From days 14 to 28, an accumulation was observed in the lungs, reaching a peak signal at 21 days following BLM administration. Thus, between 7 and 14 days, a transition phase characterized by fibroproliferation, in which mesenchymal, inflammatory, and epithelial cells activate fibrotic repair pathways, and established fibrosis occurs at 3 weeks post-induction. After 28 days, the fibrotic changes slightly decreased (Fig. 3C). Since collagen deposition indicates increased stiffness in the ECM, remodeling of the lung architecture, and deterioration of lung functions [29], we considered correlating these findings with a parameter of lung damage through the Ashcroft scale. It assigns different fibrosis scores by evaluating histological sections stained with Masson's trichrome. As reported in Fig. 3C, analysis of the degree of fibrosis of lung sections of control animals showed a predominantly normal lung architecture. At 7 days, a strong increase in score was noted with mild fibrotic changes, alveolar septa with nodular formations, and single fibrotic masses. PF, with large contiguous confluent fibrotic masses, was most evident between 14 and 21 days after BLM administration and became less severe at 28 days.

Myofibroblasts, possessing contractile properties and expressing α -SMA, play a pivotal role in excessive collagen deposition and tissue remodeling [2, 32]. Thus, histological analysis of lung sections from BLM-treated mice revealed extensive α -SMA expression at all time points, suggesting strong fibroproliferation and the presence of collagen-producing areas. In control lungs, the expression of α -SMA was found exclusively around blood vessels (Fig. 3B).

To complete the BLM animal model characterization, gene expression analysis was conducted. Tumor necrosis factor alpha (TNF- α), an inflammatory cytokine also important in the initiation of fibrotic changes, has been

tested. As illustrated in Fig. 3D, no significant up-regulation of this inflammatory gene was detected. Regarding the key fibrotic markers, collagen 1a1 (COL 1a1) and fibronectin 1 (FN1) [2, 33], crucial in ECM composition, were also assessed (Fig. 3D). In this context, a diverse gene expression modulation pattern emerges. On day 7 post-administration, both genes showed a slight increase in expression compared to the untreated group, indicating a response to alveolar damage stimuli. At 14 days post-administration, a significant peak was observed and corresponds to the transition to the fibrotic phase characterized by fibroproliferation and ECM synthesis. This signal tended to decrease in subsequent time points. Then, a partial restoration to the physiological conditions occurred (21–28 days). Furthermore, WB analysis of total lung protein lysates from mice under each experimental condition revealed that the expression of SMAD 2/3, a marker of TGF- β 1 pathway activation and indicative of a pro-fibrotic stimulus, was increased as phosphorylated SMAD 2 (pSMAD 2) starting from day 7 post-treatment. The increase was further enhanced at day 14, and then remained stably elevated, though slightly increased compared to control, at days 21 and 28 in mice treated with 5 mg/kg BLM (Fig. 3E).

BLM dose reduction does not alter the IPF induction but reduces the animal distress of treated animals

To adhere to the principle of minimizing distress and the number of animals required for a statistically reliable sample, we aimed to identify a lower dose that can recapitulate the hallmark characteristics of the most common animal model of PF, while being less invasive compared to IT BLM administration. The data reported in this paragraph refers to the study with a single IN dose of BLM 3 mg/kg. The treatment induced a maximum weight loss of 25% in the first two weeks, followed by slow weight recovery (Fig. 4A, B). Other signs of distress in BLM-treated mice included mild piloerection, labored breathing, and decreased activity, but they maintained interaction with the environment and cage mates. The macroscopic analysis of the lungs in BLM-treated mice revealed scattered lesions within regions that appeared normal, while dark lesion areas were visible across multiple lobes, bilaterally. Plethysmography data showed that BLM-treated mice (orange line) exhibited a statistically significant increase in T_i after 7 days of treatment, along with a significant reduction in RR and an increase in V_t (Fig. 4C, E, G). These results suggest the onset of acute lung injury, characterized by increased respiratory drive and respiratory effort, which resulted in a higher V_t due to relatively preserved lung compliance, similar to the soft exudative phase of lung injury. By 21 days after low-dose BLM administration, most parameters (T_i , T_e , VE, PEE, RR, T_i/T_e) indicated partial recovery of lung

function in treated mice. The trend toward reduced inspiratory capacity and V_t , even if not statistically significant, suggests the early development of a restrictive ventilatory pattern consistent with reduced lung compliance. This observation aligns with the pathophysiological changes seen in the early stages of PF, where lung stiffening due to parenchymal remodeling limits alveolar expansion. These subtle yet clinically relevant findings indicate the onset of structural changes in the lung parenchyma, which are sufficient to alter normal respiratory mechanics. Such changes could underscore the transition from acute lung injury with relatively preserved compliance to a more chronic, fibrotic phase characterized by restrictive physiology.

Histopathology revealed at 7 days post-treatment, inflammatory cell infiltrates that persisted even in the latter time points, as highlighted in H&E sections (arrows) shown in Fig. 5A. This inflammation was constantly detected throughout the disease progression, involving the entire lung parenchyma from days 14 to 21 after BLM administration, not significantly differing from that observed in animals treated with the higher dose. The Sirius Red staining and its quantification (Fig. 5A, C) showed notable fibrosis at 21 days post-instillation. The percentage of Sirius Red-positive area was similar to that observed in animals treated with a higher dose of BLM (Fig. 3C). As expected at 28 days, the fibrotic changes tend to resolve and improve toward a more normal state of the lung parenchyma. This phenomenon is well-documented in the literature and represents one of the main differences compared to the human pathology, where PF typically does not resolve [18, 34]. Regarding the key factors involved in the inflammatory and fibrotic processes, a similar pattern was observed across all markers analyzed by immunohistochemistry (Fig. 5B) and histopathological quantification at both doses (see S.I. Figure S1A, B).

Gene expression of TNF- α , COL 1a1, and FN1 through Real-Time PCR showed a peak in COL 1a1 and FN1 expression at 14 days from BLM administration, whereas TNF- α expression peaked at day 7, although it was not significantly different from control animals (Fig. 5D). The latter result could reflect the pathogenesis of IPF, where an inflammatory phenotype with the secretion of TNF- α precedes the onset and development of fibrosis with the deposition of aberrant ECM proteins such as COL 1a1 and FN1. A similar upregulation of pSMAD 2 expression found with the higher dose was observed in mice treated with 3 mg/kg BLM, at day 7 (Fig. 5E). These results showed significant lung impairment by IN administration of 3 mg/kg BLM, suggesting that this protocol has the potential to finely tune the extent of fibrosis and the degree of lung impairment, with reduced animal distress.

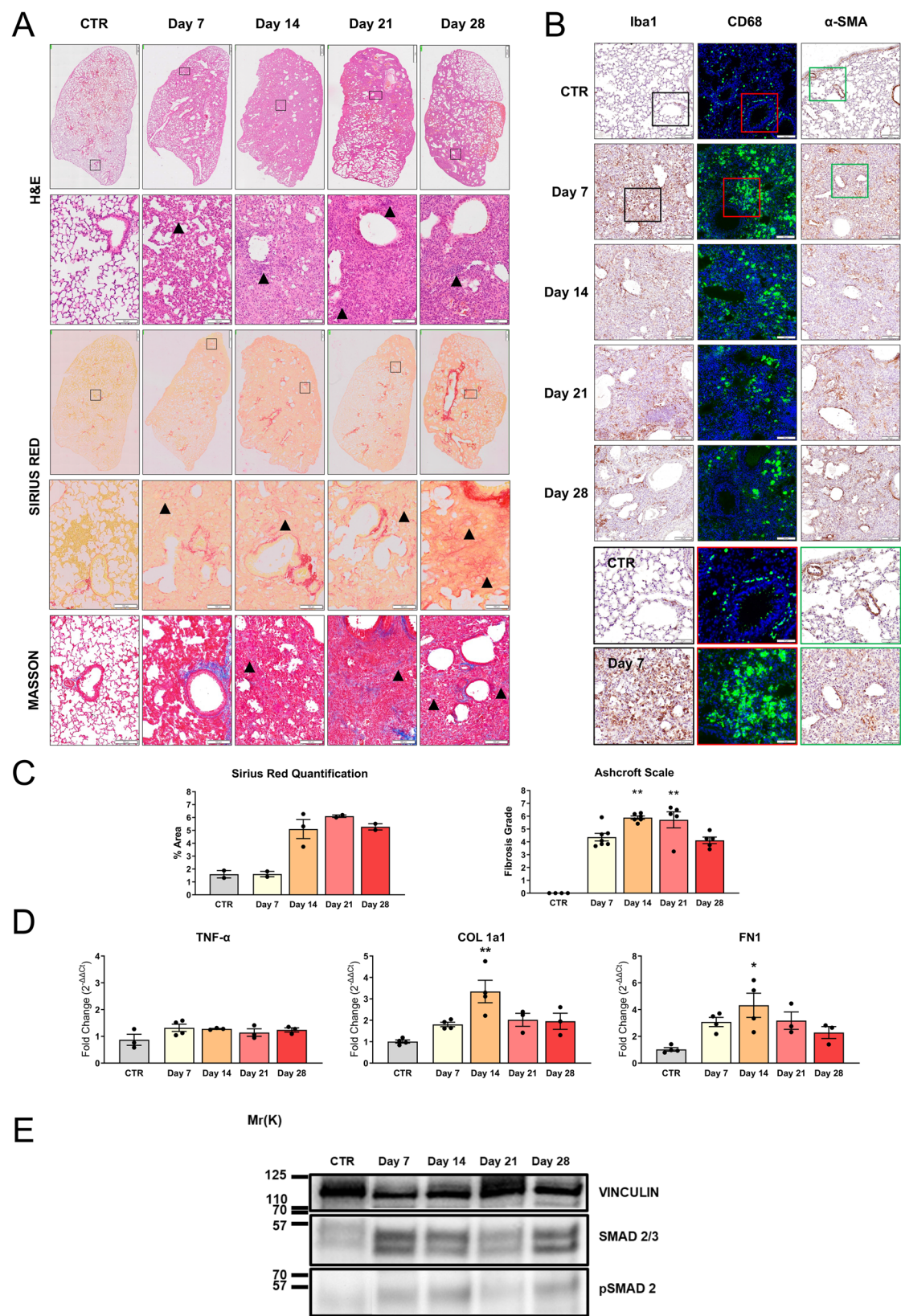


Fig. 3 (See legend on next page.)

(See figure on previous page.)

Fig. 3 Histopathological characterization in BLM-treated animals (IN—5 mg/kg). **A**) Histopathological evaluation by H&E staining (upper panel), Sirius Red staining (middle panel), and Masson's trichrome (lower panel) of lungs of vehicle mice (CTR) or treated with BLM after a single IN administration. Representative images of lung sections of animals sacrificed at 7, 14, 21, and 28 days after the treatment are reported. Scale bar=500 μ m (upper panel) – 100 μ m (lower panels). **B**) IHC for Iba1 (left panel), CD68 (green—middle panel), and α -SMA staining (right panel) of lungs of CTR or treated with BLM. Representative images of lung sections of animals sacrificed at 7, 14, 21, and 28 days after the treatment are reported, scale bar=100 μ m. The boxed areas (Iba1 black, CD68 red, α -SMA green) in CTR and day 7 sections are shown at higher magnification in the right panel, scale bar=50 μ m. **C**) Histopathological quantification of Sirius Red staining in lung section (left graph) and representation of Ashcroft scale grade (right graph) obtained by Masson's trichrome analysis of lungs of CTR or treated with BLM. Data are reported as mean \pm SE. The data were analyzed by Kruskal–Wallis test followed by Dunn's test. Significant differences compared to the CTR are reported, $**p \leq 0.01$. **D**) mRNA expression of TNF- α , COL 1a1, and FN1 was evaluated by RT-qPCR in the lungs of mice ($n=3$ per group) treated with BLM and sacrificed at different time points. Genes were normalized on β -ACT, and the $2^{-\Delta\Delta C_t}$ method was employed for relative quantification on an external calibrator. Data are reported as mean \pm SE and were analyzed with Kruskal–Wallis test followed by Dunn's test. Significant differences compared to the CTR are reported, $*p \leq 0.05$, $**p \leq 0.01$. **E**) SMAD 2/3 and pSMAD 2 expression in the lungs from CTR mouse at days 7, 14, 21, and 28 of treatment obtained with WB

Further BLM dose reduction to improve animal welfare does not induce IPF

In line with the objectives of this study to develop a reliable animal model while adhering to the principles of the 3Rs, and based on the results presented in the previous paragraphs, the final step involved a further reduction in the BLM dose. The same experimental scheme used previously was followed with a dose of 1 mg/kg of BLM. Except for a slight weight loss in the first week in BLM-treated mice, a similar trend was observed between the two groups. The treatment caused a maximum weight loss of 10% during the first week, followed by rapid recovery. Notably, from day 14 after administration, there was a full restoration to normal weight, followed by a physiological weight gain (Fig. 6A, B). The functional analysis using the plethysmograph did not highlight any significant alterations in many respiratory parameters (Te, Vt, VE, PEF, and Ti/Te), except for a reduction in RR exclusively at 7 days post-administration. This finding aligns with an adaptive response characterized by decreased RR and increased respiratory effort, as reflected by elevated PIF shortly after the injury.

Discussion

Although significant progress has been made in recent decades in alternative approaches like the use of vertebrates, such as computational studies, organoids, invertebrates, and high-resolution non-invasive imaging, there are still many aspects that require their extensive use. However, researchers must adapt to the increasing community demands regarding the Reduction, Replacement, and Refinement of in vivo analysis techniques. The present study aimed to refine the method with careful attention to animal welfare and select the BLM doses that can provide a reliable animal model resembling the main characteristics and clinical heterogeneity of human IPF. It is important to remember that an exact model reflecting human IPF has yet to be established, due to the unknown etiology of the disease. In this context, all results obtained from the BLM animal model must be carefully interpreted, taking into account that PF in these models lacks key

hallmarks of the human disease [11, 18]. On this basis, our model summarizes the common molecular mechanisms observed in the animal models of IPF, exhibiting typical signs of the human disease, such as pathophysiological changes in the respiratory parameters, modulation of fibrotic genes, and collagen fiber deposition. The IT approach represents the standard procedure but can necessitate both intubation and a nose cone or additional ketamine sedation, together with isoflurane anesthesia. This method requires a surgical incision of the trachea, which is associated with considerable peri-operative mortality and post-surgery monitoring. As a result, this protocol is more invasive and stressful for the animals, and it demands highly qualified professionals to perform the procedure [19, 35]. Moreover, the direct instillation of BLM induced strong damage to lung epithelial and endothelial cells, not comparable to the human fibrotic onset and progression [22]. To optimize the protocol for establishing the preclinical animal model and to minimize animal suffering, we investigated IN administration as an alternative route. The nasal instillation of 50 μ l of fluid in mice resulted in greater relative accumulation and persistence in the lungs [36]. Additionally, the presence of deeper anesthesia could affect the relative distribution of intranasally instilled substances, potentially facilitating their deposition within the more distal segments of the lungs [35, 36].

MALDI-TOF MS analysis demonstrated that IN instillation of BLM effectively reaches the lung, allowing its diffusion throughout the lung parenchyma and leading to the pathological changes described in the Results section and commonly reported in preclinical studies. BLM preferentially targets the lungs, due to the low expression of bleomycin hydrolase, the enzyme responsible for its metabolism; however, its effects are not limited to this organ but can also include skin redness, blistering, and tenderness [12, 13]. The anatomical connection between the nasal cavity and the gastrointestinal tract may allow gastrointestinal adsorption of BLM, but its deposition was transient, suggesting rapid clearance or metabolism in these tissues. Moreover, as reported in the literature,

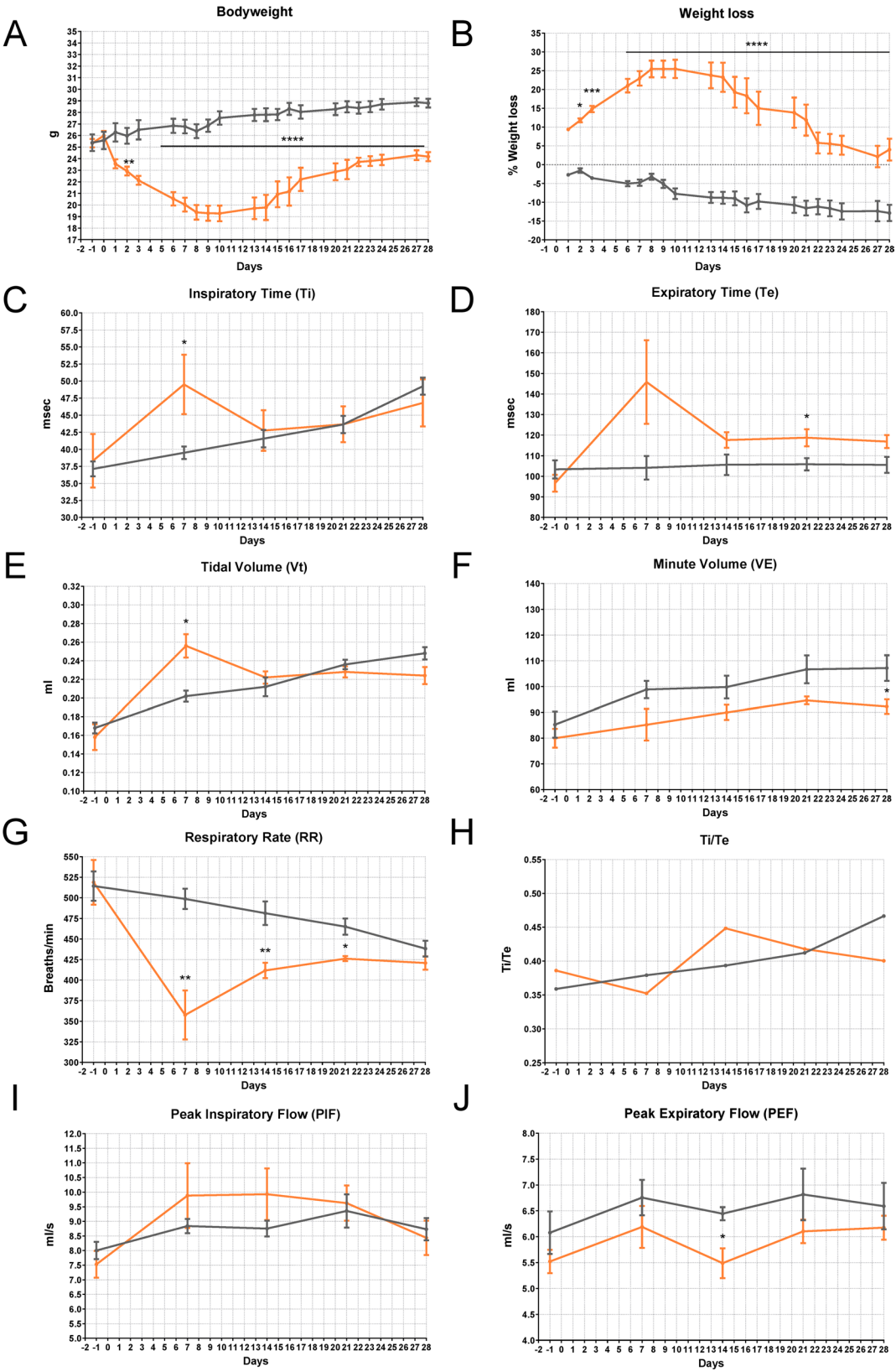


Fig. 4 (See legend on next page.)

(See figure on previous page.)

Fig. 4 Health status in BLM-induced lung injury mouse model—Plethysmography (IN—3 mg/kg). **A** Bodyweight and **B** weight loss in C57BL/6 J mice treated via single IN administration with BLM (orange line) or vehicle (grey line). The data were analyzed using Two-Way ANOVA followed by Šidák's test. * $p \leq 0.05$, ** $p \leq 0.01$, *** $p \leq 0.001$, **** $p \leq 0.0001$. **C–J** Effect of BLM on Ti (msec), Te (msec), Vt (ml), VE (ml), RR (breaths/min), Ti/Te, PIF (ml/s), and PEF (ml/s) in C57BL/6 J mice. Control animals are represented by the grey line ($n = 5$); BLM-treated animals are represented by the orange line ($n = 5$). Data are reported as mean \pm SE. The data were analyzed using the nonparametric Mann–Whitney U test comparing the parameters with the CTR group at each time point, * $p \leq 0.05$, ** $p \leq 0.01$

BLM is predominantly eliminated via renal excretion in the first 24 h [13]. Furthermore, IN instillation may promote a more uniform drug distribution due to gravity and passive inhalation. This method could represent a practical approach that partially mimics the physiological exposure to environmental agents potentially inhaled by humans. With the selection of BLM dosage and anesthesia conditions, we successfully established a phenotype that recapitulates the key features of PF observed in widely used protocols, while employing a less invasive and technically demanding induction protocol. Furthermore, the selected method has the advantage of inducing the pathology with a single treatment, further minimizing stress.

In terms of dosage, 3 mg/kg of BLM induced respiratory distress similar to that obtained with the higher dosage but with a lower weight loss (25% with respect to 30% in animals treated with 5 mg/kg). Observation from previously conducted experiments showed that high dosage caused acute lethality within the first week post-treatment in 3.5% of tested animals (data obtained from 90 observed mice from different studies, data not shown). Although this percentage is limited, it becomes significant when considering its potential impact on the development of protocols for use in preclinical model studies. Moreover, at 28 days, the percentage of recovery was more evident in low-dose-treated mice (5%), indicating better health status and improved animal welfare in line with the Refinement of the 3Rs principles. Indeed, behavioral observations should be considered when assessing pain status in mice. It was observed in BLM-treated mice, the presence of indicators of pain (hunched posture, inactivity, and moderate dyspnea). To obtain a reliable animal model that reflects the most common features of human pathology but, at the same time, considers the improvement of animal welfare, it is necessary to adopt a multimodal approach integrating observational, functional, and histopathological analyses. The results obtained during monitoring of the weight and behavior of the animals were confirmed by plethysmography. In general, the respiratory parameters recorded with both doses showed a similar trend regarding the pulmonary impairment typical of acute respiratory distress syndrome. PF reduces lung compliance and increases airway resistance, making it harder for the lungs to expand and necessitating a

slower breathing pattern to minimize the work of breathing. This is further influenced by vagal activation, which modifies the neural regulation of breathing to optimize gas exchange. Additionally, expiration becomes prolonged due to increased elastic recoil and resistance, lengthening the total breathing cycle and reducing RR. It was noted on day 7 a transient increase in Vt, particularly in the high-dose group. This finding is not typically reported in classical BLM models, and this observation may reflect a phase-specific physiological response. In the early stages of lung injury (as day 7 represents), before established fibrosis impairs lung mechanics, animals exhibit increased respiratory drive and effort, associated with prolonged Ti. This may lead to increased Vt, especially in the context of relatively preserved compliance and severe inflammation. As such, this finding is not a hallmark of fibrotic mechanics per se, but rather a dynamic adaptation during the acute phase of injury, prior to the development of overt restrictive physiology. Indeed, by days 14–21, the trend in Vt reverses toward normalization or reduction, in line with the progression of fibrosis and stiffening of the lung parenchyma. These changes collectively serve as an energy-conserving mechanism while maintaining ventilation under the mechanically compromised conditions of fibrotic lungs [37].

For a precise evaluation of lung architecture and pathological state, histology processing was performed. While inflation fixation is widely recognized as the preferred method for preserving lung morphology, this approach was not employed in the present study. Instead, lungs were divided into different lobes and processed using various methods to enable multiple downstream analyses on the same animal. However, inflation fixation generally provides superior preservation, and this should be considered a limitation of the study. The histopathological analysis revealed that a single IN dose of BLM induces a rapid development of injury and acute inflammation, followed by a chronic inflammatory phase with the initiation of fibrosis over the subsequent weeks. The high expression of lung infiltrates in the BLM group indicates that inflammation strongly contributes to the disease progression in the experimental model. In many lung diseases, both cutaneous and chronic inflammation can lead to moderate necrosis of the lung epithelia or trigger Epithelial-to-Mesenchymal Transition. Both processes, whether occurring independently or simultaneously, are

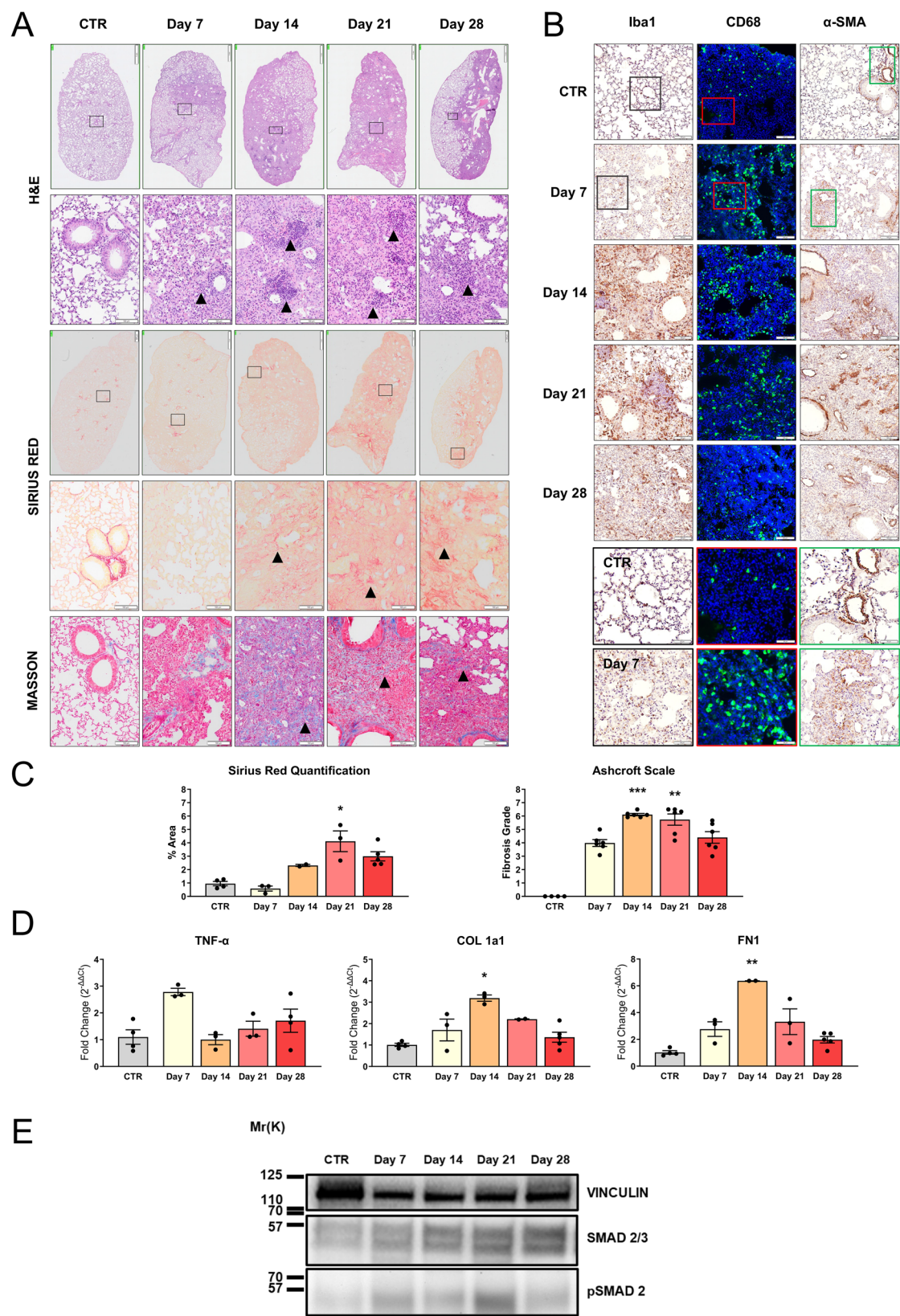


Fig. 5 (See legend on next page.)

(See figure on previous page.)

Fig. 5 Histopathological characterization in BLM-treated animals (IN—3 mg/kg). **A** Histopathological evaluation by H&E staining (upper panel), Sirius Red staining (middle panel), and Masson's trichrome (lower panel) of lungs of vehicle mice (CTR) or treated with BLM after a single IN administration. Representative images of lung sections of animals sacrificed at 7, 14, 21, and 28 days after the treatment are reported. Scale bar=500 μ m (upper panel) – 100 μ m (lower panels). **B** IHC for Iba1 (left panel), CD68 (green—middle panel), and α -SMA staining (right panel) of lungs of CTR or treated with BLM. Representative images of lung sections of animals sacrificed at 7, 14, 21, and 28 days after the treatment are reported. Scale bar=100 μ m. The boxed areas (Iba1 black, CD68 red, α -SMA green) in CTR and day 7 sections are shown at higher magnification in the right panel, scale bar=50 μ m. **C** Histopathological quantification of Sirius Red staining in lung section (left graph) and representation of Ashcroft scale grade (right graph) obtained by Masson's trichrome analysis of lungs of CTR or treated with BLM. Data are reported as mean \pm SE. The data were analyzed by Kruskal–Wallis test followed by Dunn's test. Significant differences compared to the CTR are reported, * $p \leq 0.05$, ** $p \leq 0.01$, *** $p \leq 0.001$. **D** mRNA expression of TNF- α , COL 1a1, and FN1 was evaluated by RT-qPCR in the lungs of mice ($n=3$ per group) treated with BLM and sacrificed at different time points. Genes were normalized on β -actin, and the $2^{-\Delta\Delta C_t}$ method was employed for relative quantification on an external calibrator. Data are reported as mean \pm SE and were analyzed with Kruskal–Wallis test followed by Dunn's test. Significant differences compared to the CTR are reported, * $p \leq 0.05$, ** $p \leq 0.01$. **E** SMAD 2/3 and pSMAD 2 expression in the lungs from CTR mouse at days 7, 14, 21, and 28 of treatment obtained with WB

closely associated with the development of a pathognomonic fibrotic pattern of these forms, contributing to the chronicity of the pathological state. For both doses (3 and 5 mg/kg), the percentage of Sirius Red positive collagen, H&E staining, and Ashcroft scale show a similar trend. The inflammatory/fibrotic state appears to be comparable between the two doses and analogous to the human pathological condition. An increase in α -SMA expression was observed at all time points for both BLM doses. Quantification of α -SMA-positive cells in animals treated with 3 or 5 mg/kg of BLM revealed comparable percentages within the lung parenchyma for both groups (see S.I., Figure S1A). These findings confirm the successful establishment of lung fibrosis in mice, with no significant differences between the two selected doses. CD68-positive cells were abundantly present in the lung parenchyma in both conditions, exhibiting a pronounced amoeboid morphology indicative of an activated state. Quantification of the average size of macrophages in animals treated with either BLM dose showed no statistically significant differences between the two groups (see S.I., Figure S1B).

Regarding the gene expression analyses, both doses showed a peak in the fibrotic markers (COL 1a1 and FN1) at day 14, consistent with the known time course of BLM-induced fibrosis development [38, 39]. In both treatment groups, it was detected through WB analysis the phosphorylated form of SMAD 2 which is the active type that modulates transcriptional activity. The increase in pSMAD 2 levels preceded the subsequent upregulation of FN1 and COL 1A1 (at day 7), suggesting an early role for pSMAD 2 in initiating and driving the fibrotic response promoted by the TGF- β 1 signalling [40]. No significant difference in TNF- α expression was observed between treated and control animals at either dose. However, even though it was not statistically significant, an increase in TNF- α expression was observed in animals treated with 3 mg/kg of BLM 7 days post-instillation. These data suggest a marked and prolonged inflammatory injury [41], leading to a fibrotic response at both BLM doses. It is known that key factors involved in pathogenesis are activated at the gene level during specific phases

of disease progression, so it is extremely important to evaluate their upregulation or downregulation for determining the experimental plan and, therefore, the clinical intervention. The possibility of intervening in a specific phase, targeting either inflammatory or fibrotic markers, can influence the potential therapeutic strategy's success. Despite the limitations of animal models for studying IPF, these findings highlight that both high and low doses of BLM can produce features that recapitulate the human disease. In terms of applying the principles of the 3Rs, it is unethical to administer high doses of BLM when the same effects can be achieved with a lower dose, causing less distress to the animal.

To enhance compliance, an induction dose of 1 mg/kg BLM was evaluated. This dose, like the previous ones, was selected based on protocols reported in the literature. Our functional analyses showed no significant differences in respiratory parameters or behavioral signs of distress observed previously. The rapid recovery of these parameters suggests that the initial changes were not sufficient to cause significant parenchymal structural alterations or long-term lung damage. Based on these data, the selected low dose of BLM was not effective in inducing the disease, making this model defective under the experimental conditions used. Consequently, no further analyses were conducted.

The present work is an accurate characterization, but several endpoints could be exploited in future studies to test the efficacy of therapeutic approaches or improve non-invasive methods of diagnosis and peripheral markers discovery. Despite their critical importance, age- and sex-related factors remain underexplored in animal models of IPF, highlighting a significant gap in our understanding of disease mechanisms and therapeutic responses. Moreover, lifestyle factors such as physical performance and exercise tolerance, which can modulate the resilience of lung repair systems, are frequently overlooked, further limiting the translational relevance of experimental findings [42]. A significant challenge in IPF drug development is the frequent failure of experimental therapies to replicate promising preclinical results in clinical settings. This may be attributed to in vivo models

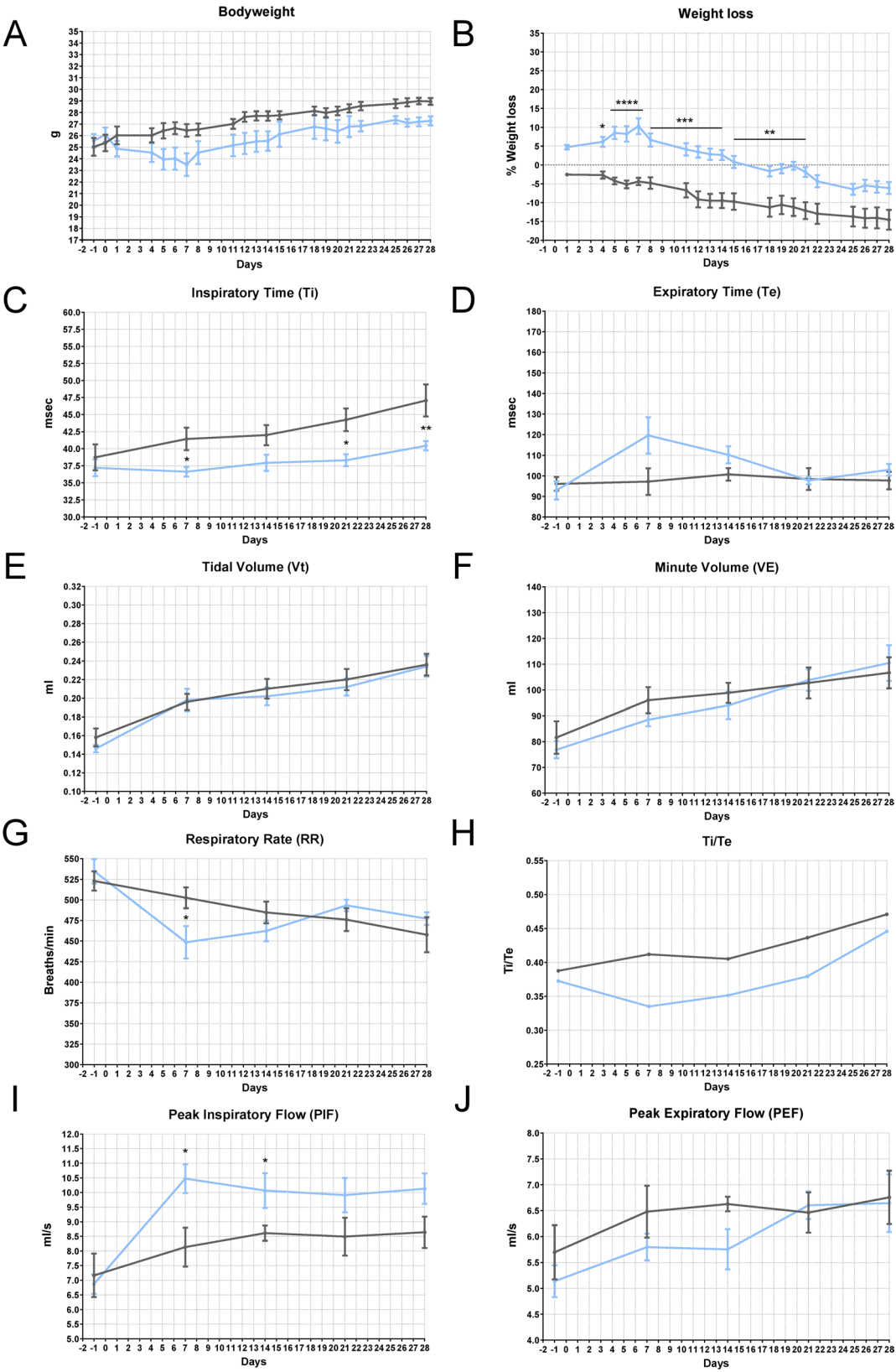


Fig. 6 (See legend on next page.)

(See figure on previous page.)

Fig. 6 Health status in BLM-induced lung injury mouse model—Plethysmography (IN—1 mg/kg). **A**) Bodyweight and **B**) weight loss in C57BL/6 J mice treated via single IN administration with BLM (light blue line) or vehicle (grey line). The data were analyzed using Two-Way ANOVA followed by Šidák's test. * $p \leq 0.05$, ** $p \leq 0.01$, *** $p \leq 0.001$, **** $p \leq 0.0001$. **C–J**) Effect of BLM on Ti (msec), Te (msec), Vt (ml), VE (ml), RR (breaths/min), Ti/Te, PIF (ml/s), and PEF (ml/s) in C57BL/6 J mice. Control animals are represented by the grey line ($n=5$); BLM-treated animals are represented by the light blue line ($n=5$). The data were analyzed using the nonparametric Mann–Whitney U test comparing the parameters with the CTR group at each time point, * $p \leq 0.05$, ** $p \leq 0.01$

that inadequately reflect the pathophysiological and structural complexity of IPF. Factors such as age-related lung remodeling and sex-specific differences further complicate drug distribution and efficacy, underscoring the need for more representative preclinical frameworks to bridge the translational gap. To address the unmet therapeutic needs in lung fibrotic disorders, the inclusion of these underrepresented variables in our proposed approach may lead to effective clinical results for this debilitating disease.

Conclusions

This research provides a well-validated and comparable animal model with the gold standard (IT administration) for further elucidating the underlying mechanisms of lung fibrosis pathogenesis and evaluating potential therapeutic targets for lung disorders. A single IN administration of 3 mg/kg of BLM in deeply anesthetized subjects is preferred to achieve the aforementioned purposes. In addition, a strong emphasis was given to the Refinement of the procedures, not only for ethical purposes but also for the obtainment of reliable and reproducible scientific data [43]. Compromised animal health status can result in low-quality data, reduced reproducibility, and limited translational relevance to humans. Moreover, the failure of an experiment to yield benefits to either humans or animals constitutes, in itself, an animal welfare concern. Designing experiments focusing on future reproducibility leads to a more informative animal model for research in the field of veterinary medicine, biomedical science, and public health.

Abbreviations

PF	Pulmonary fibrosis
ILDs	Interstitial lung diseases
ECM	Extracellular matrix
IPF	Idiopathic pulmonary fibrosis
BLM	Bleomycin
IT	Intratracheal
IN	Intranasal
MALDI-TOF MS	Matrix-assisted laser desorption/ionization time-of-flight mass spectrometry
RR	Respiratory rate
Ti	Inspiratory time
Te	Expiratory time
PIF	Peak inspiratory flow
PEF	Peak expiratory flow
Vt	Tidal volume
VE	Minute volume
H&E	Hematoxylin-eosin
Iba1	Ionized calcium-binding adaptor molecule 1
α -SMA	Alpha smooth muscle actin
RT-PCR	Reverse-transcriptase PCR

SE	Standard error of the mean
ANOVA	Analysis of variance
TNF- α	Tumor necrosis factor alpha
COL 1a1	Collagen 1a1
FN1	Fibronectin 1

Supplementary Information

The online version contains supplementary material available at <https://doi.org/10.1186/s12890-025-04001-4>.

Supplementary Material 1.

Acknowledgements

The authors gratefully acknowledge Recordati SpA for providing the plethysmograph instrumentation and Dr. Marco Gobbi, Head of Laboratory of Pharmacodynamics and Pharmacokinetics, Mario Negri Institute for Pharmacological Research IRCCS, Milano, Italy, for his contribution to the statistical analysis. The graphical abstract was created in BioRender. <https://BioRender.com/7tf8weh>.

Authors' contributions

Conceptualization AS, PB, AM; Data curation AS, AM; Formal analysis AS, AVS, GR, AC, AM; Funding acquisition PB, Investigation AS, AVS, GYM, GR, AC, AM; Methodology AS, AM; Project administration PB; Resources AS, PB, AM; Supervision PB, EC, RT; Validation AS, PB, AM; Visualization AS, PB, AM; Writing original draft AS, AVS, PB, RT, AM; Writing review & editing AS, AVS, PB, RT, AM. All authors read and approved the final manuscript.

Funding

This research was supported by EU funding within the NextGenerationEU-MUR PNRR Extended Partnership initiative on Emerging Infectious Diseases (Project no. PE00000007, INF-ACT).

Data availability

All data generated or analyzed during this study are included in this published article.

Declarations

Ethics approval and consent to participate

The Mario Negri Institute for Pharmacological Research IRCCS adheres to the principles outlined in the following laws, regulations, and directives concerning the care and use of laboratory animals: Italian law (D.lgs 26/2014; Authorization No. 19/2008-A issued on March 6, 2008 by the Ministry of Health); the Mario Negri Institutional Regulations and Policies—which provide internal authorization for persons conducting animal experiments (Quality Management System Certificate, UNI EN ISO 9001:2015, Reg. No. 6121); the NIH Guide for the Care and Use of Laboratory Animals (2011 edition); and the EU Directives and Guidelines (EEC Council Directive 2010/63/UE). This work was reviewed by the IRCCS-IRFMN Animal Care and Use Committee (IACUC) and subsequently approved by the Italian "Istituto Superiore di Sanità" (Code: 558/2021-PR).

Consent for publication

Not applicable.

Competing interests

The authors declare no competing interests.

Author details

¹Department of Biochemistry and Molecular Pharmacology, Laboratory of Nanobiology and Nanotoxicology, Mario Negri Institute for Pharmacological Research IRCCS, Milan, Italy

²Department of Medical and Surgical Sciences, Respiratory Disease Unit, University Hospital of Modena, University of Modena and Reggio Emilia, Modena, Italy

³Department of Medical and Surgical Sciences for Children & Adults, Laboratory of Cell Therapies and Respiratory Medicine, University of Modena and Reggio Emilia, Modena, Italy

⁴Molecular and Regenerative Medicine PhD Program, University of Modena Reggio Emilia, Modena, Italy

⁵Department of Biochemistry and Molecular Pharmacology, Laboratory of Pharmacodynamics and Pharmacokinetics, Mario Negri Institute for Pharmacological Research IRCCS, Milan, Italy

Received: 24 January 2025 / Accepted: 17 October 2025

Published online: 24 November 2025

References

- Cottin V, Hirani NA, Hotchkiss DL, Nambiar AM, Ogura T, Otaola M, et al. Presentation, diagnosis and clinical course of the spectrum of progressive-fibrosing interstitial lung diseases. *Eur Respir Rev*. 2018;27:180076. <https://doi.org/10.1183/16000617.0076-2018>.
- Wilson MS, Wynn TA. Pulmonary fibrosis: pathogenesis, etiology and regulation. *Mucosal Immunol*. 2009;2:103–21. <https://doi.org/10.1038/mi.2008.85>.
- Richeldi L, Collard HR, Jones MG. Idiopathic pulmonary fibrosis. *Lancet*. 2017;389:1941–52. [https://doi.org/10.1016/S0140-6736\(17\)30866-8](https://doi.org/10.1016/S0140-6736(17)30866-8).
- Wijnsbeek M, Suzuki A, Maher TM. Interstitial lung diseases. *Lancet*. 2022;400:769–86. [https://doi.org/10.1016/S0140-6736\(22\)01052-2](https://doi.org/10.1016/S0140-6736(22)01052-2).
- Wijnsbeek M, Cottin V. Spectrum of Fibrotic Lung Diseases. Drazen JM, editor. *N Engl J Med*. 2020;383:958–68. <https://doi.org/10.1056/NEJMra2005230>.
- Samet JM, Coultas D, Raghu G. Idiopathic pulmonary fibrosis: tracking the true occurrence is challenging. *Eur Respir J*. 2015;46:604–6. <https://doi.org/10.1183/13993003.00958-2015>.
- Moore BB, Hogaboam CM. Murine models of pulmonary fibrosis. *American Journal of Physiology-Lung Cellular and Molecular Physiology*. 2008;294:L152–60. <https://doi.org/10.1152/ajplung.00313.2007>.
- Christensen PJ, Goodman RE, Pastoriza L, Moore B, Toews GB. Induction of lung fibrosis in the mouse by intratracheal instillation of fluorescein isothiocyanate is not T-cell-dependent. *Am J Pathol*. 1999;155:1773–9. [https://doi.org/10.1016/S0002-9440\(10\)65493-4](https://doi.org/10.1016/S0002-9440(10)65493-4).
- McDonald S, Rubin P, Chang AYC, Penney DP, Finkelstein JN, Grossberg S, et al. Pulmonary changes induced by combined mouse β -interferon (rMuIFN- β) and irradiation in normal mice — toxic versus protective effects. *Radiother Oncol*. 1993;26:212–8. [https://doi.org/10.1016/0167-8140\(93\)90262-7](https://doi.org/10.1016/0167-8140(93)90262-7).
- O'Dwyer DN, Moore BB. Animal Models of Pulmonary Fibrosis. In: Alper S, Janssen WJ, editors. *Lung Innate Immunity and Inflammation* [Internet]. New York, NY: Springer New York; 2018 [cited 2024 Mar 19]. p. 363–78. https://doi.org/10.1007/978-1-4939-8570-8_24.
- B. Moore B, Lawson WE, Oury TD, Sisson TH, Raghavendran K, Hogaboam CM. Animal Models of Fibrotic Lung Disease. *Am J Respir Cell Mol Biol*. 2013;49:167–79. <https://doi.org/10.1165/rcmb.2013-0094TR>.
- Liu T, De Los Santos FG, Phan SH. The Bleomycin Model of Pulmonary Fibrosis. In: Rittié L, editor. *Fibrosis* [Internet]. New York, NY: Springer New York; 2017 [cited 2023 Aug 14]. p. 27–42. https://doi.org/10.1007/978-1-4939-7113-8_2.
- Della Latta V, Cecchetti A, Del Ry S, Morales MA. Bleomycin in the setting of lung fibrosis induction: from biological mechanisms to counteractions. *Pharmacol Res*. 2015;97:122–30. <https://doi.org/10.1016/j.phrs.2015.04.012>.
- Li S, Shi J, Tang H. Animal models of drug-induced pulmonary fibrosis: an overview of molecular mechanisms and characteristics. *Cell Biol Toxicol*. 2022;38:699–723. <https://doi.org/10.1007/s10565-021-09676-z>.
- Froudarakis M, Hatzimichael E, Kyriazopoulou L, Lagos K, Pappas P, Tzanos AG, et al. Revisiting bleomycin from pathophysiology to safe clinical use. *Crit Rev Oncol Hematol*. 2013;87:90–100. <https://doi.org/10.1016/j.critrevonc.2012.12.003>.
- Bayer RA, Gaynor ER, Fisher RI. Bleomycin in non-Hodgkin's lymphoma. *Semin Oncol*. 1992;19:46–52 discussion 52–53.
- Wang L, Wang Y, Yang T, Guo Y, Sun T. Angiotensin-converting enzyme 2 attenuates bleomycin-induced lung fibrosis in mice. *Cell Physiol Biochem*. 2015;36:697–711. <https://doi.org/10.1159/000430131>.
- Moeller A, Ask K, Warburton D, Gaudie J, Kolb M. The bleomycin animal model: a useful tool to investigate treatment options for idiopathic pulmonary fibrosis? *Int J Biochem Cell Biol*. 2008;40:362–82. <https://doi.org/10.1016/j.biocel.2007.08.011>.
- Tashiro J, Rubio GA, Limper AH, Williams K, Elliot SJ, Ninou I, et al. Exploring animal models that resemble idiopathic pulmonary fibrosis. *Front Med*. 2017;4:118. <https://doi.org/10.3389/fmed.2017.00118>.
- Driscoll KE. Intratracheal instillation as an exposure technique for the evaluation of respiratory tract toxicity: uses and limitations. *Toxicol Sci*. 2000;55:24–35. <https://doi.org/10.1093/toxsci/55.1.24>.
- Khadangi F, Forgues A-S, Tremblay-Pitre S, Dufour-Mailhot A, Henry C, Boucher M, et al. Intranasal versus intratracheal exposure to lipopolysaccharides in a murine model of acute respiratory distress syndrome. *Sci Rep*. 2021;11:7777. <https://doi.org/10.1038/s41598-021-87462-x>.
- Savin IA, Zenkova MA, Sen'kova AV. Pulmonary fibrosis as a result of acute lung inflammation: molecular mechanisms, relevant in vivo models, prognostic and therapeutic approaches. *IJMS*. 2022;23:14959. <https://doi.org/10.3390/ijms232314959>.
- Gul A, Yang F, Xie C, Du W, Mohammadtursun N, Wang B, et al. Pulmonary fibrosis model of mice induced by different administration methods of bleomycin. *BMC Pulm Med*. 2023;23:91. <https://doi.org/10.1186/s12890-023-0234-9-z>.
- Zubair F. MALDI mass spectrometry based proteomics for drug discovery & development. *Drug Discov Today Technol*. 2021;40:29–35. <https://doi.org/10.1016/j.ddtec.2021.09.002>.
- Milton PL, Dickinson H, Jenkin G, Lim R. Assessment of respiratory physiology of C57BL/6 mice following bleomycin administration using barometric plethysmography. *Respiration*. 2012;83:253–66. <https://doi.org/10.1159/000330586>.
- Schipke J, Brandenberger C, Rajcs A, Manninger M, Alogna A, Post H, et al. Assessment of cardiac fibrosis: a morphometric method comparison for collagen quantification. *J Appl Physiol*. 2017;122:1019–30. <https://doi.org/10.1152/japplphysiol.00987.2016>.
- Ashcroft T, Simpson JM, Timbrell V. Simple method of estimating severity of pulmonary fibrosis on a numerical scale. *J Clin Pathol*. 1988;41:467–70. <https://doi.org/10.1136/jcp.41.4.467>.
- Hübner R-H, Gitter W, Eddine El Mokhtari N, Mathiak M, Both M, Bolte H, et al. Standardized quantification of pulmonary fibrosis in histological samples. *BioTechniques*. 2008;44:507–17. <https://doi.org/10.2144/000112729>.
- Vaickus LJ, Bouchard J, Kim J, Natarajan S, Remick DG. Assessing pulmonary pathology by detailed examination of respiratory function. *Am J Pathol*. 2010;177:1861–9. <https://doi.org/10.2353/ajpath.2010.100053>.
- Maier TM. Small airways in idiopathic pulmonary fibrosis: quiet but not forgotten. *Am J Respir Crit Care Med*. 2021;204:1010–1. <https://doi.org/10.1164/rccm.202108-2007ED>.
- Tonelli R, Smit MR, Castaniere I, Casa GD, Andrisani D, Gozzi F, et al. Quantitative CT-analysis of over aerated lung tissue and correlation with fibrosis extent in patients with idiopathic pulmonary fibrosis. *Respir Res*. 2024;25:359. <https://doi.org/10.1186/s12931-024-02970-4>.
- Barratt S, Creamer A, Hayton C, Chaudhuri N. Idiopathic pulmonary fibrosis (IPF): an overview. *JCM*. 2018;7:201. <https://doi.org/10.3390/jcm7080201>.
- Nho RS, Ballinger MN, Rojas MM, Ghadiali SN, Horowitz JC. Biomechanical force and cellular stiffness in lung fibrosis. *Am J Pathol*. 2022;192:750–61. <https://doi.org/10.1016/j.ajpath.2022.02.001>.
- Ishida Y, Kuninaka Y, Mukaida N, Kondo T. Immune mechanisms of pulmonary fibrosis with bleomycin. *IJMS*. 2023;24:3149. <https://doi.org/10.3390/ijms24043149>.
- Seo Y, Qiu L, Magnen M, Conrad C, Moussavi-Harami SF, Looney MR, et al. Optimizing anesthesia and delivery approaches for dosing into lungs of mice. *bioRxiv*. 2023;2023.02.01.526706. <https://doi.org/10.1101/2023.02.01.526706>.
- Southam DS, Dolovich M, O'Byrne PM, Inman MD. Distribution of intranasal instillations in mice: effects of volume, time, body position, and anesthesia. *Am J Physiol-Lung Cell Mol Physiol*. 2002;282:L833–9. <https://doi.org/10.1152/ajplung.00173.2001>.
- Marchioni A, Tonelli R, Cerri S, Castaniere I, Andrisani D, Gozzi F, et al. Pulmonary stretch and lung mechanotransduction: implications for progression in the fibrotic lung. *IJMS*. 2021;22:6443. <https://doi.org/10.3390/ijms22126443>.

38. Izbicki G, Segel MJ, Christensen TG, Conner MW, Breuer R. Time course of bleomycin-induced lung fibrosis. *Int J Exp Pathol*. 2002;83:111–9. <https://doi.org/10.1046/j.1365-2613.2002.00220.x>.
39. Swaisgood CM, French EL, Noga C, Simon RH, Ploplis VA. The development of Bleomycin-induced pulmonary fibrosis in mice deficient for components of the fibrinolytic system. *Am J Pathol*. 2000;157:177–87. [https://doi.org/10.1016/S0002-9440\(10\)64529-4](https://doi.org/10.1016/S0002-9440(10)64529-4).
40. Gu L, Zhu Y, Yang X, Guo Z-J, Xu W, Tian X. Effect of TGF- β /smad signaling pathway on lung myofibroblast differentiation. *Acta Pharmacol Sin*. 2007;28:382–91. <https://doi.org/10.1111/j.1745-7254.2007.00468.x>.
41. Boehme JD, Pietkiewicz S, Lavrik I, Jeron A, Bruder D. Erratum to: Morphological and functional alterations of alveolar macrophages in a murine model of chronic inflammatory lung disease. *Lung*. 2015;193:955–955. <https://doi.org/10.1007/s00408-015-9812-9>.
42. Badenes-Bonet D, Rodó-Pin A, Castillo-Villegas D, Vicens-Zygmunt V, Bermudo G, Hernández-González F, et al. Predictors and changes of physical activity in idiopathic pulmonary fibrosis. *BMC Pulm Med*. 2022;22:340. <https://doi.org/10.1186/s12890-022-02134-4>.
43. Voelkl B, Altman NS, Forsman A, Forstmeier W, Gurevitch J, Jaric I, et al. Author correction: reproducibility of animal research in light of biological variation. *Nat Rev Neurosci*. 2020;21:394–394. <https://doi.org/10.1038/s41583-020-0326-y>.

Publisher's Note

Springer Nature remains neutral with regard to jurisdictional claims in published maps and institutional affiliations.